

Spin-Imbalanced Pairing and Fermi Surface Deformation in Flat Bands

Kukka-Emilia Huhtinen,^{*} Marek Tylutki,^{*} Pramod Kumar, Tuomas I. Vanhala, Sebastiano Peotta, and Päivi Törmä[†]
Department of Applied Physics, Aalto University, 00076 Aalto, Finland
 (Dated: June 21, 2022)

We study the attractive Hubbard model with spin imbalance on two lattices featuring a flat band: the Lieb and kagome lattices. We present mean-field phase diagrams featuring exotic superfluid phases, similar to the Fulde-Ferrell-Larkin-Ovchinnikov (FFLO) state, whose stability is confirmed by dynamical mean-field theory (DMFT). The nature of the pairing is found to be qualitatively different from the Fermi surface shift responsible for the usual FFLO state. The presence of a flat band allows for changes in the particle momentum distributions at null energy cost. This facilitates formation of nontrivial superfluid phases via multiband Cooper pair formation: the momentum distribution of the spin component in the flat band deforms to mimic the Fermi surface of the other spin component residing in a dispersive band. The Fermi surface of the unpaired particles that are typical for gapless superfluids becomes deformed as well. The results highlight the profound effect of flat dispersions on Fermi surface instabilities, and provide a potential route for observing spin-imbalanced superfluidity and superconductivity.

Interactions in fermion systems may cause Fermi surface instabilities, for instance towards pairing [1] or symmetry-breaking deformations of the Fermi surface, called the Pomeranchuk instability (PI) [2]. These mechanisms lead to various phases of matter such as both conventional and high- T_c superconductivity [3–5], topological phases thereof [6], the two superfluid phases of different symmetry in ^3He [7] or superfluidity in lattice systems of ultracold fermions predicted by the Hubbard model [8], including models with spin-orbit coupling [9, 10]. In the repulsive Hubbard model, the superfluidity may coexist with the magnetic stripe order [11], or with PI as in Refs. [12, 13]. Spin-imbalanced superfluidity, on the other hand, has been predicted to simultaneously display pairing, superfluidity, and gapless excitations (Fermi surfaces). These exotic phases of matter spontaneously break symmetries of the system, for instance rotational or translational, in addition to the breaking of the $U(1)$ gauge symmetry characteristic of any BCS-type superfluid. In the FFLO state [14, 15] the Cooper pairs carry a finite momentum. Deformed Fermi surface superfluidity (DFS) [16, 17] has been proposed as another alternative that gives a lower energy than the conventional BCS theory. Such predictions have remained elusive, supported only by indirect experimental evidence [18, 19]. Phase separation, instead of exotic spin-imbalanced superfluids, has been observed in ultracold quantum gases [20–24]; this is consistent with predictions for continuum systems [25–27], although theory suggests that lattice systems may stabilize the FFLO state due to nesting [28–33]. In general, singularities in the density of states (DOS) are known to enhance Fermi surface instabilities. Here we show that multiband lattice systems which possess the ultimate DOS singularity, namely a flat (constant) en-

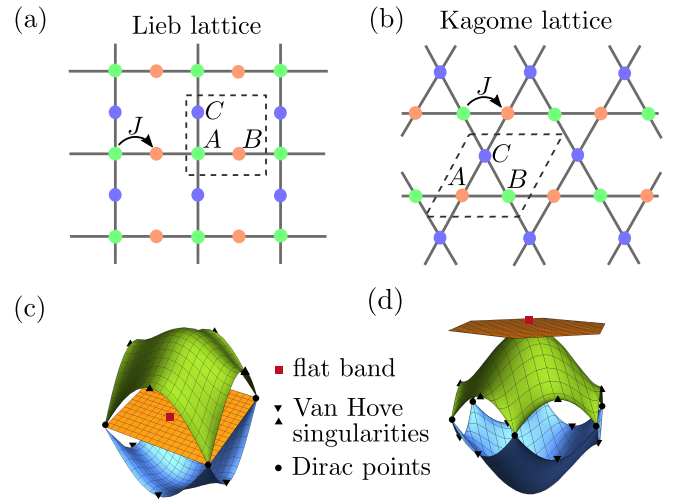


FIG. 1: Two lattice geometries featuring a flat band: (a) a Lieb lattice and (b) a kagome lattice. The elementary cells are delimited with dashed lines. Three sites that constitute an elementary cell are labeled as A, B and C. Below, single-particle band structures of these lattices: (c) Lieb and (d) kagome with two dispersive bands and one flat band. The latter is indicated with a red square. Black triangles show van Hove singularities, i.e. points where the density of states (DOS) diverges. Dirac points with vanishing DOS are marked by black dots. The singularities and Dirac points are shown in Fig. 2 with lines.

ergy band, allow deformations of the particle momentum distribution without energy cost and thereby stabilize a new type of spin-imbalanced superfluidity. We find that the origin of the pairing is different from a simple minority particle Fermi surface shift conventionally responsible for FFLO states.

We study two examples of a Hubbard model with a flat band in the single-particle energy spectrum: a Lieb lattice and a kagome lattice Hubbard model. Both lat-

^{*}These authors contributed equally to this work.

[†]Electronic address: paivi.torma@aalto.fi

tices have three sublattices and feature two dispersive bands and a flat band. The lattices and the band structures are shown in Fig 1. Importantly, such lattices have been experimentally realized for ultracold gases [34–36], in designer lattices made by atomistic control [37, 38], in optical analogues [39, 40] and also implementations with superconducting circuits have been proposed theoretically [41]. We choose to fix chemical potentials and therefore consider the grand-canonical ensemble. The real-space grand-canonical Hamiltonian reads

$$H = \sum_{\sigma} \sum_{\alpha, \beta} \psi_{i\alpha\sigma}^{\dagger} \mathcal{H}_{i\alpha, j\beta} \psi_{j\beta\sigma} - \sum_{\sigma} \mu_{\sigma} N_{\sigma} + H_{\text{int}}, \quad (1)$$

where the lattice information is contained in the single-particle Hamiltonian $\mathcal{H}_{i\alpha, j\beta}$ responsible for hopping between the lattice sites, α and β are the sublattice (orbital) indices. In our model, we consider only nearest neighbour hopping for both lattices. The particle number operator is defined as $N_{\sigma} = \sum_{i\alpha} \psi_{i\alpha\sigma}^{\dagger} \psi_{i\alpha\sigma}$, and the on-site interaction enters as $H_{\text{int}} = U \sum_{i\alpha} \psi_{i\alpha\uparrow}^{\dagger} \psi_{i\alpha\downarrow}^{\dagger} \psi_{i\alpha\downarrow} \psi_{i\alpha\uparrow}$. Upon defining the average chemical potential as $\mu = (\mu_{\uparrow} + \mu_{\downarrow})/2$ and the effective magnetic field as $h = (\mu_{\uparrow} - \mu_{\downarrow})/2$, the particle number term can be rewritten as $\sum_{\sigma} \mu_{\sigma} N_{\sigma} = \mu N + hM$, where N is the total particle number and $M = N_{\uparrow} - N_{\downarrow}$ the total magnetization. By J , which we also use as the unit of energy, we denote the hopping strength between the neighbouring lattice sites. Hereafter the lattice constant a is assumed $a = 1$.

The BCS (mean-field) approximation of the Hamiltonian (1) introduces a pairing field $\Delta_{i\alpha} = U \langle \psi_{i\alpha\downarrow} \psi_{i\alpha\uparrow} \rangle$, where the average denotes a ground state expectation value at zero temperature and a grand-canonical average $\langle \mathcal{O} \rangle = \text{Tr}(\mathcal{O} e^{-\beta H}) / \text{Tr} e^{-\beta H}$ at finite temperatures $k_B T = 1/\beta$ (k_B is the Boltzmann constant). We allow for an imbalance in chemical potentials, $\mu_{\uparrow} \neq \mu_{\downarrow}$, so the particles in a Cooper pair may have a nonzero center-of-mass momentum \mathbf{q} . This is reflected by the Fulde-Ferrell (FF) ansatz for the pairing field, $\Delta_{j\alpha} = \Delta_{\alpha} e^{i\mathbf{q} \cdot \mathbf{j}}$. Since we assume our system to be translationally invariant, we change the basis to the quasi-momentum basis by performing a Fourier transform, $\psi_{j\alpha\sigma} = \sum_{\mathbf{k}} c_{\mathbf{k}\alpha\sigma} e^{i\mathbf{k} \cdot \mathbf{j}} / \sqrt{N}$. After this transformation the mean-field Hamiltonian with the FF ansatz becomes

$$H_{\text{FF}} = \sum_{\mathbf{k}} \left[\Psi_{\mathbf{k}}^{\dagger} \mathcal{H}_{\text{BdG}} \Psi_{\mathbf{k}} - 3\mu_{\downarrow} - \frac{1}{U} \text{Tr} \Delta^{\dagger} \Delta \right], \quad (2)$$

where we introduced a Nambu spinor $\Psi_{\mathbf{k}} = (c_{\mathbf{k}, A\uparrow}, c_{\mathbf{k}, B\uparrow}, c_{\mathbf{k}, C\uparrow}, c_{\mathbf{q}-\mathbf{k}, A\downarrow}^{\dagger}, c_{\mathbf{q}-\mathbf{k}, B\downarrow}^{\dagger}, c_{\mathbf{q}-\mathbf{k}, C\downarrow}^{\dagger})^T$ and the Bogoliubov-de-Gennes (BdG) Hamiltonian

$$\mathcal{H}_{\text{BdG}} = \begin{pmatrix} \mathcal{H}_{\mathbf{k}} - \mu_{\uparrow} & \Delta \\ \Delta^{\dagger} & -\mathcal{H}_{-\mathbf{k}+\mathbf{q}} + \mu_{\downarrow} \end{pmatrix}. \quad (3)$$

The pairing fields are collected into a diagonal matrix $(\Delta)_{\alpha\beta} = \Delta_{\alpha} \delta_{\alpha\beta}$.

The single-particle Hamiltonian can be diagonalized as $\mathcal{G}_{\mathbf{k}\sigma}^{\dagger} \mathcal{H}_{\mathbf{k}\sigma} \mathcal{G}_{\mathbf{k}\sigma} = \epsilon_{\mathbf{k}\sigma}$. In this single-particle band basis, the field operators take the form

$$\begin{pmatrix} \mathbf{d}_{\mathbf{k}\uparrow} \\ \mathbf{d}_{\mathbf{q}-\mathbf{k}\downarrow}^{\dagger} \end{pmatrix} = \begin{pmatrix} \mathcal{G}_{\mathbf{k}\uparrow}^{\dagger} & 0 \\ 0 & \mathcal{G}_{\mathbf{q}-\mathbf{k}\downarrow}^{\dagger} \end{pmatrix} \Psi_{\mathbf{k}}, \quad (4)$$

where the components of the collective vector $(\mathbf{d}_{\mathbf{k}\uparrow}, \mathbf{d}_{\mathbf{q}-\mathbf{k}\downarrow}^{\dagger})^T$ correspond to different bands. A further unitary transformation to quasi-particle basis, $(\gamma_{\mathbf{k}, \mathbf{q}\uparrow}, \gamma_{\mathbf{k}, \mathbf{q}\downarrow}^{\dagger})^T$, diagonalizes the full BdG Hamiltonian, \mathcal{H}_{BdG} . The diagonalized Hamiltonian reads $H_{\text{FF}} = \sum_{\mathbf{k}} (\gamma_{\mathbf{k}, \mathbf{q}\uparrow}^{\dagger} \mathbf{E}_{\mathbf{k}, \mathbf{q}\uparrow} \gamma_{\mathbf{k}, \mathbf{q}\uparrow} + \gamma_{\mathbf{k}, \mathbf{q}\downarrow}^{\dagger} \mathbf{E}_{\mathbf{k}, \mathbf{q}\downarrow} \gamma_{\mathbf{k}, \mathbf{q}\downarrow}) + \mathcal{E}$, where $\mathbf{E}_{\mathbf{k}, \mathbf{q}\sigma}$ are diagonal matrices of the quasi-particle energies, and the energy offset $\mathcal{E} = \sum_{\mathbf{k}} (-3\mu_{\downarrow} + \text{Tr} \Delta^{\dagger} \Delta / U - \text{Tr} \mathbf{E}_{\mathbf{k}, \mathbf{q}\downarrow})$. In order to find thermodynamically stable phases at finite temperature, we look for global minima of the thermodynamic potential $\Omega = -\ln \text{Tr} \exp(-\beta H_{\text{FF}}) / \beta$, which can be calculated as $\Omega = -\sum_{\mathbf{k}, \sigma} \text{Tr} \ln[1 + \exp(-\beta \mathbf{E}_{\mathbf{k}, \mathbf{q}\sigma})] / \beta + \mathcal{E}$. We minimize it with respect to all components of Δ and \mathbf{q} independently. For each thus obtained configuration we can calculate the densities as $n_{\mathbf{k}\alpha\sigma} = \langle c_{\mathbf{k}\alpha\sigma}^{\dagger} c_{\mathbf{k}\alpha\sigma} \rangle$.

We present mean field phase diagrams in Fig. 2 for both considered lattices, at interaction $U = -4J$ and temperature $k_B T = 0.1J$. Due to particle-hole symmetry, the phase diagram for the Lieb lattice is symmetric with respect to the axis $\mu = (\mu_{\uparrow} + \mu_{\downarrow})/2 = 0$. This symmetry is absent in the kagome lattice. We assume $\mu_{\uparrow} \geq \mu_{\downarrow}$. In both cases, the BCS phase is favored for sufficiently low chemical potential imbalance $h = (\mu_{\uparrow} - \mu_{\downarrow})/2$. As h is increased, the phase switches to either a normal phase, or to nonuniform superfluidity with nonzero \mathbf{q} . We distinguish two such phases: the FF and η phase. In the FF region, \mathbf{q} grows until it reaches the boundary of the Brillouin zone (BZ). The phase is then referred to as the η -pairing phase [43, 44], or simply η phase in the following. In the Lieb lattice, a third imbalanced superfluid phase with $\mathbf{q} = 0$, the so-called Sarma phase [45–48], is found at large imbalance h . The focus of this Letter is on the FF and η phases, and the Sarma phase will be discussed in detail in [49].

In both lattices, we find that the DOS singularities are manifested in the phase diagram. Nonuniform superfluidity occurs near crossing points of singularities, where the density of states near the Fermi surfaces of both components is large. In the Lieb lattice, flat band (FB) singularities are always involved at interaction $U = -4J$. In the kagome lattice, however, an FF region is found away from the flat band, where the minority component reaches the Van Hove (VH) singularity on the first dispersive band, and the majority component reaches that on the second dispersive band. This region is relatively small compared to the one near to the FB singularity [42].

To verify the existence of the FF phase beyond the simple mean-field approximation, we performed DMFT calu-

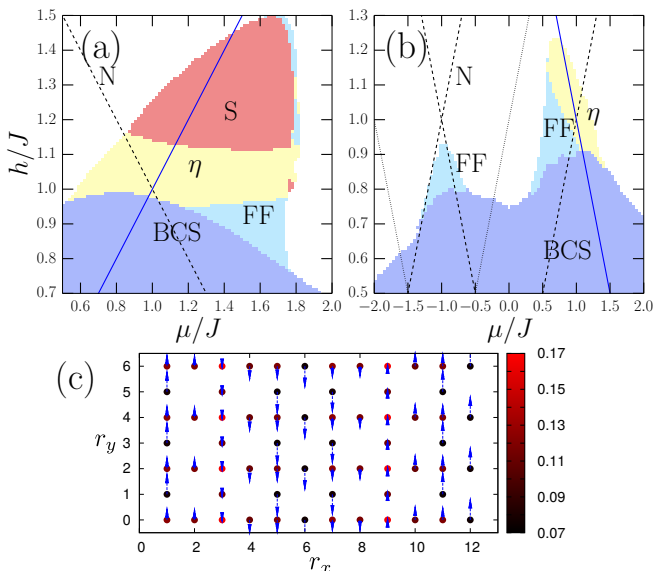


FIG. 2: Phase diagram for (a) a Lieb lattice and (b) kagome lattice at $U = -4J$ and $k_B T = 0.1J$. Here, $\mu = (\mu_\uparrow + \mu_\downarrow)/2$ and $h = (\mu_\uparrow - \mu_\downarrow)/2$. Dashed lines indicate Van Hove singularities, blue solid lines the flat bands, and dotted lines the Dirac points. They are determined as $\mu_{\uparrow,\downarrow} = E_s$, i.e. where the chemical potential reaches the energy E_s corresponding to a relevant point in the DOS. We find that nonuniform superfluidity is favored where the singularities cross. In the case of the FF phase, the amplitude of \mathbf{q} grows across the stability region until it reaches the Brillouin zone, where the phase is called the η phase. Moreover, for the Lieb lattice, we observe a stable Sarma phase at large imbalance, labeled S. (c) The s-wave order parameter, $\Delta(r_x, r_y)$ (arrow length and direction), and spin-polarization $n_s(r_x, r_y) = n_\uparrow(r_x, r_y) - n_\downarrow(r_x, r_y)$ (dots with color scale) for different positions (r_x, r_y) at $h \sim 1.40$, $\mu \sim 0.0$, $U = -6J$ and $k_B T = 0.05J$ in the FFLO state evaluated using DMFT for the Lieb lattice [42].

lations in a partial real-space formulation for both lattices (see [42] for details). We present a two dimensional profile distribution of the s-wave order parameter, $\Delta(r_x, r_y)$, and spin-polarization, $n_s(r_x, r_y) = n_\uparrow(r_x, r_y) - n_\downarrow(r_x, r_y)$, in the Lieb lattice in Fig. 2. The DMFT calculation was performed for the 18-site cluster shown in [42]. In the figure, this unit cell is stacked in the y -direction. The modulations of the order parameter and spin-polarization are a clear indication of an FFLO state. DMFT results showing an FF state in the Kagome lattice are presented in the supplementary material [42].

Importantly, one can see from Fig. 2 that the FF and η phases are stable mostly close to the flat band DOS singularity. Near the flat band the Fermi surface of one component is small, or even nonexistent and one would expect pairing to be suppressed. Indeed, in conventional BCS theory pairing is enhanced by the size of the Fermi surface. The formation of nonuniform superfluidity in our case is not explained solely by matching of the Fermi surfaces as in previous literature [31], indicating there are

other mechanisms at play.

In order to get an insight into the mechanism of pairing in these multiband systems, we look at the band resolved densities, $n_{\mathbf{k}n\sigma} = \langle d_{\mathbf{k}n\sigma}^\dagger d_{\mathbf{k}n\sigma} \rangle$, where n is the band index, that is, densities of each spin component decomposed in the band basis of the single-particle Hamiltonian. As presented in the schematic in Fig. 3(a), we find that the Fermi surface of the minority component gets shifted by a vector \mathbf{q} towards the Fermi surface of the majority component where the pairing takes place — this is the conventional mechanism behind the FFLO state [14, 15, 31]. In a square lattice, this leads to nesting which stabilizes the FFLO state [28, 31]. In our case this is *intra*-band pairing, i.e. pairing between atoms from the same band, as will be explained later. The calculated band-resolved densities are shown in Fig. 3(b) for the Lieb lattice and in Fig. 3(c) for the kagome lattice. The lower dispersive band (I-DB) remains almost completely filled (and therefore we do not plot it), while deformation of the density distributions takes place in the upper dispersive band (II-DB) in the region where the Fermi surfaces match.

An interesting effect can be observed for atoms residing in the FB. For one component they remain completely unaffected, while for the other the distribution of atoms, which was initially flat, gets deformed in such a way as to mimic the density of the first component in the II-DB. In the case of a Lieb lattice (kagome lattice) the FB remains completely filled (completely empty) for the majority (minority) component, while for the minority (majority) component the distribution of atoms gets deformed. This suggests an *inter*-band pairing between the atoms in the flat band and atoms in the upper dispersive band. This is an energetically favorable process, as the atoms in a flat band can rearrange at vanishing energy cost due to flat dispersion relation.

The excess atoms of the majority component, that do not take part in the pairing, form a normal gas. Its presence can be seen in the total density traced along the high-symmetry lines, as well as in the differences $n_{\mathbf{k}\uparrow} - n_{\mathbf{k}\downarrow}$, as shown in Fig. 4 for both lattices. The density profiles of the paired components are matched up to a shift by a constant; for some momenta \mathbf{k} there is a jump in the densities of the two components. This is due to the presence of a normal gas. Since, as is stated by Luttinger's theorem, the number of available states inside the Fermi sphere does not change upon interactions, this constant shift is $n_{\mathbf{k}\uparrow} - n_{\mathbf{k}\downarrow} = 1$, see Ref. [31]. This mechanism can be seen also in the band-resolved densities in Figs. 3(a), (b). The presence of the normal gas in the upper dispersive band gives rise to an observable Fermi surface seen as sharp density jumps. Even though the normal component does not participate in the pairing, its Fermi surface is deformed by the pairing mechanism of the other atoms [42].

To gain further understanding of the nature of pairing, we study pairing correlations between different bands,

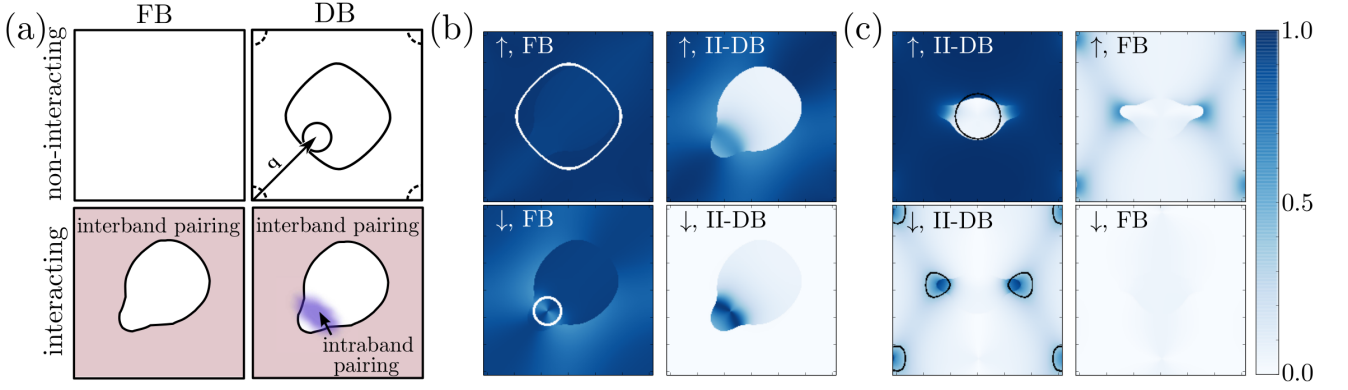


FIG. 3: (a) The FF pairing mechanism in a multiband system with a flat band. The Fermi surface of the minority component shifts towards the Fermi surface of the majority component by the momentum \mathbf{q} . Both intra- and interband pairings (regions which are shown here in color) contribute to the overall effect. The calculated band-resolved density profiles $n_{\mathbf{k}n\sigma}$ in (b) the Lieb lattice for $\mu = 1.4J$ and $h = 0.9J$ and in (c) the kagome lattice for $\mu = 0.6J$ and $h = 0.9J$ demonstrate the discussed scenario. Continuous lines indicate the noninteracting Fermi surfaces. Note that in the case of the Lieb lattice, the minority component FS is centred around the M point of the BZ (in the corners), and the momentum \mathbf{q} shifts it towards the Γ point. FB stands for a flat band, and II-DB for the upper dispersive band, shown in Fig. 1 in orange and green respectively.

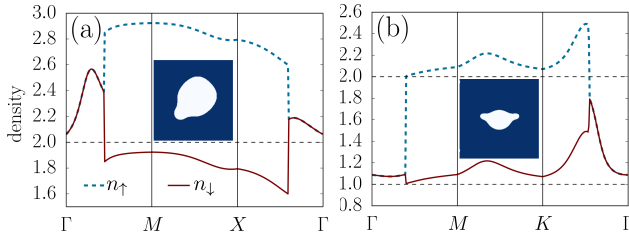


FIG. 4: Densities along high symmetry lines in (a) the Lieb and (b) the kagome lattice. Coinciding densities indicate complete pairing, whereas a jump in density $n_{\mathbf{k}\uparrow} - n_{\mathbf{k}\downarrow} = 1$ arises due to the presence of a normal gas characteristic for spin-imbalanced superfluids. The region where this unpaired component resides, clear from the difference in the densities $n_{\mathbf{k}\uparrow} - n_{\mathbf{k}\downarrow}$, is shown as insets for both cases, respectively. Dark blue (white) corresponds to a value of one (zero): around the boundaries of the BZ, the system hosts both paired and normal components, while particles near the Γ point are completely paired.

$\langle d_{\mathbf{k}n\uparrow} d_{(\mathbf{q}-\mathbf{k})m\downarrow} \rangle$, where n and m are band indices. As can be seen in Figs. 5(a),(b), the lattices feature both intra- and interband pairing. Intraband pairing occurs mostly between particles on II-DB, and is most pronounced in the region where the Fermi surfaces match. This is similar to what is found in the square lattice, where particles on the same energy band can pair due to the shift of one Fermi surface by \mathbf{q} . The Fermi surface of the normal component is reflected also in the pairing correlations, and intraband pairing within II-DB is completely absent in the region where the unpaired particles reside. The other prominent pairing is between particles on the FB and those on II-DB. Again, the Fermi surface of the normal component is visible as sharp jumps between low and

high correlations. Contrary to intraband pairing, this interband pairing occurs mostly where the unpaired gas lies, and the paired components occupy different energy bands. Pairing is made possible in this situation by the possibility of atoms on the FB to readjust their density profile to mimic that of the other component on II-DB at low energy cost.

Correlations between other bands, albeit smaller, are also present. In particular, also particles of the majority (minority) component on the flat band contribute to pairing in the Lieb (kagome) lattice. Moreover, the various pairings give further indication that the unpaired particles are distributed among different bands.

Interband pairing is also found without the contribution of the flat band in the FF region of the kagome lattice located at $\mu = -1$ (see [42]). In that region, it is due to both components being near a Van Hove singularity, leading to two nearly hexagonal Fermi surfaces, as well as a high density of states. However, as the particle distributions are different, the pairing in that case is limited to a small region of the BZ, in contrast to the high correlations found almost everywhere when the flat band is involved.

While other possibilities also exist [37–41], ultracold quantum gases may offer the most immediate realization of our predictions. Lieb and kagome geometries have already been realized by optical lattices [34–36] and novel techniques such as digital mirror devices and holograms [50–52] allow further flexibility. The on-site interaction used here is feasible by the use of Feshbach resonances. Our mean-field calculations give critical temperatures $k_B T_c$ from around $0.2J$ to $0.5J$ [49]. In 2D, the Berezinskii-Kosterlitz-Thouless (BKT) temperature for superfluidity is typically smaller than the BCS one

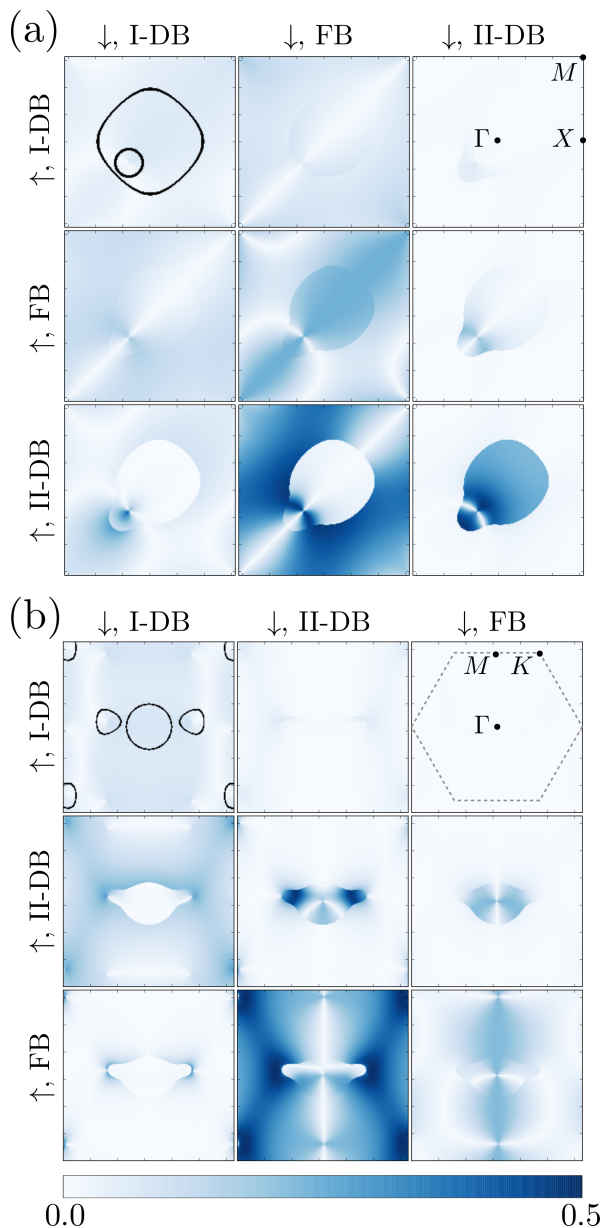


FIG. 5: Pairing $\langle d_{\mathbf{k}n\uparrow}d_{(\mathbf{q}-\mathbf{k})m\downarrow} \rangle$ between different bands in (a) the Lieb lattice and (b) the kagome lattice. In both lattices one can clearly see the pairing correlation strengths for different pairings. Most pairing takes place as intraband pairing in the II-DB and as interband pairing between the FB and the II-DB. Top right panels also show the positions of high-symmetry points of the Brillouin zones. Dashed lines in (b) indicate the boundary of the Brillouin zone.

but can be of the same order of magnitude [53–55]. Deformations and nontrivial pairing correlations may appear in these flat band systems already well above the critical temperature, which is an interesting topic of future study.

In summary, we studied the attractive Hubbard model on the Lieb and kagome lattices, both featuring a flat band. We found with both mean-field and DMFT meth-

ods that the FFLO phase can be stable. When one component partially fills the flat band, the mechanisms explaining the formation of this phase involve intra- and interband pairing. The former occurs between particles on the same dispersive band, and is most pronounced in the region where Fermi surfaces are matched due to the finite momentum of the Cooper pairs. This is similar to the previous predictions of the FFLO state in various models [31]. In contrast, the interband pairing occurs between particles on the flat band and on a dispersive band. This pairing is made possible by the constant dispersion relation of the flat band, leading to a low energy cost of deformation of the particle momentum distribution. Particles on the flat band can therefore mirror the distribution of particles on dispersive bands, thus enhancing the pairing. This mechanism of spin-imbalanced pairing is strikingly different from the conventional minority Fermi surface shift (and nesting in lattices). Flat band singularities are known to enhance magnetism [56–58] and superfluidity [53–55, 59–63]; here we have shown that, in the case of spin-imbalanced pairing, it not only enhances interactions but also makes the pairing mechanism qualitatively different from the case of dispersive bands. Since experimental preparation of artificial lattice quantum systems is advancing rapidly [8, 38, 64], our predictions on the stability of the FFLO pairing in flat band lattices may show the route to direct observation of spin-imbalanced pairing and superfluidity.

Acknowledgements.— This work was supported by the Academy of Finland through its Centres of Excellence Programme (2012-2017) and under project NOs. 284621, 303351 and 307419, and by the European Research Council (ERC-2013-AdG-340748-CODE). This project has received funding from the European Unions Horizon 2020 research and innovation programme under the Marie Skłodowska-Curie Grant Agreement No. 702281 (FLATOPS). T.I.V. acknowledges support from the Väisälä foundation. Computing resources were provided by CSC – the Finnish IT Centre for Science and the Triton cluster at Aalto University.

-
- [1] L. N. Cooper, *Phys. Rev.* **104**, 1189 (1956).
 - [2] I. I. Pomeranchuk, *JETP* **8**, 361 (1959).
 - [3] J. G. Bednorz and K. A. Müller, *Zeitschrift für Physik B Condensed Matter* **64**, 189 (1986).
 - [4] P. A. Lee, N. Nagaosa, and X.-G. Wen, *Rev. Mod. Phys.* **78**, 17 (2006).
 - [5] I. Bloch, J. Dalibard, and W. Zwerger, *Rev. Mod. Phys.* **80**, 885 (2008).
 - [6] M. Sato and Y. Ando, *Reports on Progress in Physics* **80**, 076501 (2017).
 - [7] A. J. Leggett, *Rev. Mod. Phys.* **47**, 331 (1975).
 - [8] P. Törmä and K. Sengstock, *Quantum Gas Experiments: Exploring Many-Body States* (World Scientific Publishing Co, 2015).

- [9] M. Iskin, *Phys. Rev. A* **88**, 013631 (2013).
- [10] C. Qu, Z. Zheng, M. Gong, Y. Xu, L. Mao, X. Zou, G. Guo, and C. Zhang, *Nature Communications* **4**, 2710 (2013).
- [11] T. I. Vanhala and P. Törmä, ArXiv e-prints (2017), [arXiv:1708.06749](#).
- [12] M. L. Kiesel, C. Platt, and R. Thomale, *Phys. Rev. Lett.* **110**, 126405 (2013).
- [13] M. Kitatani, N. Tsuji, and H. Aoki, *Phys. Rev. B* **95**, 075109 (2017).
- [14] P. Fulde and R. A. Ferrell, *Phys. Rev.* **135**, A550 (1964).
- [15] A. Larkin and Y. Ovchinnikov, *JETP* **20**, 762 (1965).
- [16] H. Müther and A. Sedrakian, *Phys. Rev. Lett.* **88**, 252503 (2002).
- [17] A. Sedrakian, J. Mur-Petit, A. Polls, and H. Müther, *Phys. Rev. A* **72**, 013613 (2005).
- [18] R. Casalbuoni and G. Nardulli, *Rev. Mod. Phys.* **76**, 263 (2004).
- [19] Y.-a. Liao, A. S. C. Rittner, T. Paprotta, W. Li, G. B. Partridge, R. G. Hulet, S. K. Baur, and E. J. Mueller, *Nature* **467**, 567 EP (2010).
- [20] M. W. Zwierlein, A. Schirotzek, C. H. Schunck, and W. Ketterle, *Science* **311**, 492 (2006).
- [21] G. B. Partridge, W. Li, R. I. Kamar, Y.-a. Liao, and R. G. Hulet, *Science* **311**, 503 (2006).
- [22] G. B. Partridge, W. Li, Y. A. Liao, R. G. Hulet, M. Haque, and H. T. C. Stoof, *Phys. Rev. Lett.* **97**, 190407 (2006).
- [23] Y. Shin, C. H. Schunck, A. Schirotzek, and W. Ketterle, *Nature* **451**, 689 (2008).
- [24] S. Nascimbène, N. Navon, K. J. Jiang, L. Tarruell, M. Teichmann, J. McKeever, F. Chevy, and C. Salomon, *Phys. Rev. Lett.* **103**, 170402 (2009).
- [25] D. E. Sheehy and L. Radzihovsky, *Phys. Rev. Lett.* **96**, 060401 (2006).
- [26] D. E. Sheehy and L. Radzihovsky, *Annals of Physics* **322**, 1790 (2007).
- [27] A. Recati, C. Lobo, and S. Stringari, *Phys. Rev. A* **78**, 023633 (2008).
- [28] T. K. Koponen, T. Paananen, J.-P. Martikainen, and P. Törmä, *Phys. Rev. Lett.* **99**, 120403 (2007).
- [29] M. J. Wolak, B. Grémaud, R. T. Scalettar, and G. G. Batrouni, *Phys. Rev. A* **86**, 023630 (2012).
- [30] J. E. Baarsma and P. Törmä, *Journal of Modern Optics* **63**, 1795 (2016).
- [31] J. J. Kinnunen, J. Baarsma, J.-P. Martikainen, and P. Törmä, *Reports on Progress in Physics* (also [arXiv:1706.07076](#)) (2018).
- [32] A. Cichy and A. Ptok, ArXiv e-prints (2017), [arXiv:1710.06395](#).
- [33] M. O. J. Heikkinen, D.-H. Kim, M. Troyer, and P. Törmä, *Phys. Rev. Lett.* **113**, 185301 (2014).
- [34] G.-B. Jo, J. Guzman, C. K. Thomas, P. Hosur, A. Vishwanath, and D. M. Stamper-Kurn, *Phys. Rev. Lett.* **108**, 045305 (2012).
- [35] S. Taie, H. Ozawa, T. Ichinose, T. Nishio, S. Nakajima, and Y. Takahashi, *Science Advances* **1** (2015), [10.1126/sciadv.1500854](#).
- [36] H. Ozawa, S. Taie, T. Ichinose, and Y. Takahashi, *Phys. Rev. Lett.* **118**, 175301 (2017).
- [37] M. R. Slot, T. S. Gardenier, P. H. Jacobse, G. C. P. van Miert, S. N. Kempkes, S. J. M. Zevenhuizen, C. M. Smith, D. Vanmaekelbergh, and I. Swart, *Nat Phys* **13**, 672 (2017).
- [38] R. Drost, T. Ojanen, A. Harju, and P. Liljeroth, *Nat Phys* **13**, 668 (2017).
- [39] S. Mukherjee, A. Spracklen, D. Choudhury, N. Goldman, P. Öhberg, E. Andersson, and R. R. Thomson, *Phys. Rev. Lett.* **114**, 245504 (2015).
- [40] R. A. Vicencio, C. Cantillano, L. Morales-Inostroza, B. Real, C. Mejía-Cortés, S. Weimann, A. Szameit, and M. I. Molina, *Phys. Rev. Lett.* **114**, 245503 (2015).
- [41] X.-H. Deng, C.-Y. Lai, and C.-C. Chien, *Phys. Rev. B* **93**, 054116 (2016).
- [42] See supplementary material for details on the DMFT methods, DMFT results in the kagome lattice, discussion of the second FF region in the kagome lattice and details on the Fermi surface deformation close to the FB singularity in the Lieb lattice.
- [43] C. N. Yang, *Phys. Rev. Lett.* **63**, 2144 (1989).
- [44] A. Ptok, A. Cichy, K. Rodríguez, and K. J. Kapcia, *Phys. Rev. A* **95**, 033613 (2017).
- [45] G. Sarma, *J. Phys. Chem. Solids* **24**, 1029 (1963).
- [46] W. V. Liu and F. Wilczek, *Phys. Rev. Lett.* **90**, 047002 (2003).
- [47] L. He and P. Zhuang, *Phys. Rev. B* **79**, 024511 (2009).
- [48] D.-H. Kim, J. S. J. Lehtikainen, and P. Törmä, *Phys. Rev. Lett.* **110**, 055301 (2013).
- [49] M. Tylutki and P. Törmä, to be published (2018).
- [50] K. Hueck, A. Mazurenko, N. Luick, T. Lompe, and H. Moritz, *Review of Scientific Instruments* **88**, 016103 (2017), <https://doi.org/10.1063/1.4973969>.
- [51] G. Gauthier, I. Lenton, N. M. Parry, M. Baker, M. J. Davis, H. Rubinsztein-Dunlop, and T. W. Neely, *Optica* **3**, 1136 (2016).
- [52] P. Zupancic, P. M. Preiss, R. Ma, A. Lukin, M. E. Tai, M. Rispoli, R. Islam, and M. Greiner, *Opt. Express* **24**, 13881 (2016).
- [53] S. Peotta and P. Törmä, *Nat. Comm.* **6**, 8944 (2015).
- [54] A. Julku, S. Peotta, T. I. Vanhala, D.-H. Kim, and P. Törmä, *Phys. Rev. Lett.* **117**, 045303 (2016).
- [55] L. Liang, T. I. Vanhala, S. Peotta, T. Siro, A. Harju, and P. Törmä, *Phys. Rev. B* **95**, 024515 (2017).
- [56] A. Mielke, *Journal of Physics A: Mathematical and General* **25**, 4335 (1992).
- [57] H. Tasaki, *Phys. Rev. Lett.* **69**, 1608 (1992).
- [58] A. Mielke and H. Tasaki, *Comm. Math. Phys.* **158**, 341 (1993).
- [59] V. A. Khodel and V. R. Shaginyan, *JETP* **51**, 553 (1990).
- [60] V. Khodel, V. Shaginyan, and V. Khodel, *Physics Reports* **249**, 1 (1994).
- [61] T. T. Heikkilä, N. B. Kopnin, and G. E. Volovik, *JETP Letters* **94**, 233 (2011).
- [62] N. B. Kopnin, T. T. Heikkilä, and G. E. Volovik, *Phys. Rev. B* **83**, 220503 (2011).
- [63] D. Yamamoto, C. Sato, T. Nikuni, and S. Tsuchiya, *Phys. Rev. Lett.* **110**, 145304 (2013).
- [64] S. Kuhr, *National Science Review* **3**, 170 (2016).

Supplementary Material: Spin-Imbalanced Pairing and Fermi Surface Deformation in Flat Bands

DYNAMICAL MEAN-FIELD THEORY

Dynamical mean-field theory (DMFT) maps a lattice problem to an effective single impurity problem taking into account the lattice effects in a self-consistent manner. A central quantity is the self-energy $\Sigma_{ij}(i\omega_n)$, where i and j index the lattice sites and $\omega_n = \pi(2n+1)T$, where T is the temperature, are the Matsubara frequencies. Within single-site DMFT the self-energy is assumed to be local to each site i and uniform over the whole lattice, so that $\Sigma_{ij}(i\omega_n) \sim \delta_{ij}\Sigma(i\omega_n)$. For inhomogeneous states such as the Fulde-Ferrell-Larkin-Ovchinnikov phase (FFLO), however, the uniformity assumption breaks, as the order parameter can be different for different lattice sites. To study such states, we thus use a partially real-space cluster extension of DMFT [S1, S2].

More rigorously, the DMFT method in Nambu-Gorkov formalism for a given unit cell can be described as follows. The local Green's function of the lattice system limited to a single unit cell can be calculated as

$$\mathbf{G}(i\omega_n) = \frac{1}{N_k} \sum_{\mathbf{k}} (\mathbf{G}^0(\mathbf{k}, i\omega_n)^{-1} - \Sigma(i\omega_n))^{-1}, \quad (\text{S1})$$

where the bold quantities are matrices whose dimension equals the number of sites within the unit cell and N_k is the number of k -points. Each component consists of a (2×2) matrix with normal Green's functions as diagonal components, while the off-diagonal components are anomalous Green's functions. Thus the 2×2 block $\mathbf{G}(i\omega_n)_{ij}$ is the Green's function between sites i and j of the unit cell. The non-interacting Green's function $\mathbf{G}^0(\mathbf{k}, i\omega_n)^{-1}_{ij} = (i\omega_n + h)\delta_{ij}\sigma_0 + \mu\delta_{ij}\sigma_z - \mathbf{T}(\mathbf{k})_{ij}\sigma_z$, where $\mathbf{T}_{\mathbf{k}}$ is the superlattice Fourier transform of the hopping matrix. The site diagonal self-energy at the i th site is given by the following (2×2) matrix

$$\Sigma_i(i\omega_n) = \begin{pmatrix} \Sigma_i(i\omega_n) & S_i(i\omega_n) \\ S_i(i\omega_n) & -\Sigma_i^*(i\omega_n) \end{pmatrix}$$

where $\Sigma(i\omega_n)(S(i\omega_n))$ is the normal (anomalous) part of the self-energy.

For each site i in the unit cell, there is an effective single impurity Anderson model, which is defined by the dynamical Weiss mean-field

$$\mathcal{G}_i(i\omega_n)^{-1} = (\mathbf{G}(i\omega_n)_{ii})^{-1} + \Sigma_i(i\omega_n). \quad (\text{S2})$$

Given the Weiss function \mathcal{G}_i for all i , we calculate the self-energy of each of the impurity problems using a continuous time quantum Monte-Carlo (CTINT) algorithm [S3]

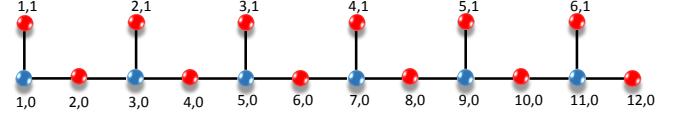


FIG. S1: Schematic diagram of the unit cell chosen for studying the FFLO order. Real space positions of the sites in the unit cell are labeled by the indices (r_x, r_y) . Sites of the same color have equivalent order parameters at half-filling.

for the Lieb lattice, and an exact diagonalization (ED) solver for the kagome lattice. These new self-energies are then used again in equation S1 and the process is iterated until a converged solution is found.

For the Lieb lattice, the calculations were performed for a unit cell of 18 sites, shown in Fig. S1. In this unit cell, the self-energy is still local but varies spatially for different sites in the unit cell, i.e. $\Sigma_{ij}(i\omega_n) = \Sigma_i(i\omega_n)\delta_{ij}$. At half-filling, it is expected that the three-site unit cell (see Fig. 1 in the main text) is sufficient to investigate the interaction-induced order parameters, while larger unit cells should be considered to capture FFLO order appearing in the spin-imbalanced case. Further we define the s-wave order parameter from the anomalous Green's function F as

$$\Delta(r_x, r_y) = UF(r_x, r_y)(\tau \rightarrow 0^-) \quad (\text{S3})$$

where (r_x, r_y) are the positions of the sites in the unit cell and τ is the imaginary time. Similarly, we denote $n_\sigma(r_x, r_y) = G(r_x, r_y, \sigma)(\tau \rightarrow 0^-)$, where G is the normal Green's function, and define the spin-polarization as

$$n_s(r_x, r_y) = n_\uparrow(r_x, r_y) - n_\downarrow(r_x, r_y). \quad (\text{S4})$$

In the kagome lattice, calculations were performed on the three-site unit cell shown in Fig. 1 in the main text. The Fulde-Ferrell (FF) ansatz $\Delta_{\mathbf{j}\alpha} = \Delta_\alpha e^{i\mathbf{q} \cdot \mathbf{j}}$ is included by performing the transformation $\psi_{\mathbf{j}\alpha\sigma} \rightarrow \psi_{\mathbf{j}\alpha\sigma} e^{-i\mathbf{q} \cdot \mathbf{r}_{\mathbf{j}}/2}$, where $\mathbf{r}_{\mathbf{j}}$ is the position of the \mathbf{j} th lattice site. The dependence on the momentum \mathbf{q} of the Cooper pairs is then included in the hopping matrices, and the non-interacting Green's function becomes $\mathbf{G}^0(\mathbf{k}, i\omega_n)^{-1}_{ij} = (i\omega_n + h)\delta_{ij}\sigma_0 + \mu\delta_{ij}\sigma_0 - \text{diag}(\mathbf{T}(\mathbf{k} + \mathbf{q}/2)_{ij}, -\mathbf{T}(\mathbf{k} - \mathbf{q}/2)_{ij}^\dagger)$, where $\mathbf{T}(\mathbf{k})$ is again the Fourier transform of the hopping matrix. Like in the Lieb lattice, the self-energy is assumed local, but can be different for the three sites in the unit cell.

The computation is performed at different amplitudes of \mathbf{q} , with the direction fixed perpendicular to one of the lattice vectors, corresponding to the most favorable direction found in mean-field calculations. The chemical potentials are tuned to achieve the same filling fractions for all different \mathbf{q} , and the most favourable amplitude is determined by comparing the total energies. The results for lattice filling fractions $n_\uparrow \approx 2.06$ and $n_\downarrow \approx 1.62$ with

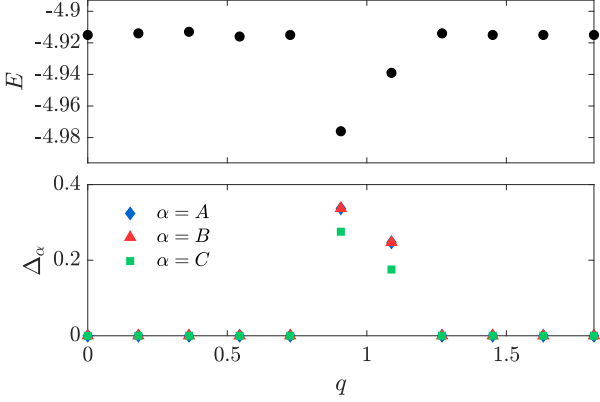


FIG. S2: (a) Total energy per unit cell and (b) order parameters computed using DMFT as a function of the amplitude of \mathbf{q} at lattice filling fractions $n_\uparrow \approx 2.06$ and $n_\downarrow \approx 1.62$, with $U = -4J$ and at zero temperature. In (b), different symbols represent the order parameters in the three sites of the unit cell. In the FF state, two of the order parameters are equal due to the symmetry of the kagome lattice, while the third is smaller than the others due to the finite momentum \mathbf{q} , which breaks the symmetry of the lattice.

interaction $U = -4J$, are shown in Fig. S2. The computation converged to a state with finite order parameters around $q \approx 1.0$, indicating an FF state. The FF state at $q \approx 0.73$ gave the lowest total energy. At these filling fractions, the majority component has reached the flat band, so these results confirm the mean-field observation that the FF state can exist near the flat-band singularity.

INTERBAND PAIRING AWAY FROM THE FLAT BAND SINGULARITY

In the kagome lattice, a region of stability of the FF phase was found around $\mu = -1$, away from the flat-band singularity. Band resolved densities and correlations are shown in Figures S3 for a point in this region. The flat band is almost completely empty for both components, and contributes little to the pairing. In contrast to what is observed for the FF phase near the flat band singularity, intraband pairing is almost absent, and interband pairing between atoms on the first and second dispersive bands dominates. This pairing occurs in the regions where the Fermi surfaces are most closely matched. It is interesting to see that, even though the Fermi surfaces are perfectly matched at zero \mathbf{q} , the FF phase is favourable. This is due to the different distributions of the components: the minority component occupies the center of the Brillouin zone, whereas the majority component occupies the corners. The momentum \mathbf{q} allows for the Fermi seas of the two components to overlap slightly, increasing the

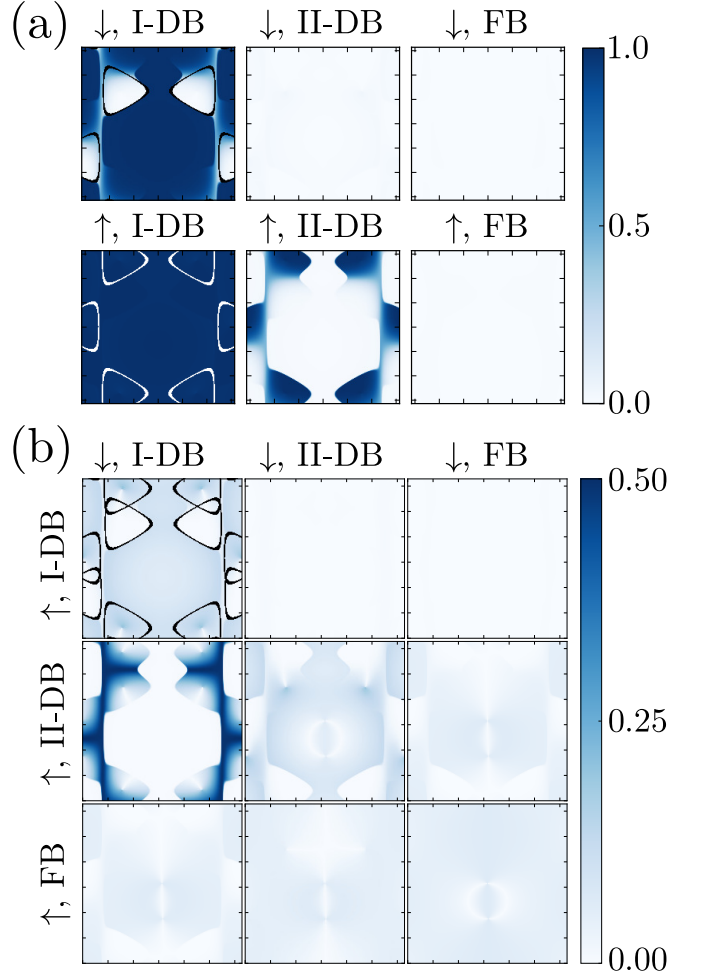


FIG. S3: (a) Band-resolved density profiles and (b) pairing $\langle d_{\mathbf{k}n\uparrow} d_{(\mathbf{q}-\mathbf{k})n\downarrow} \rangle$ in the kagome lattice at $\mu = -1.0$, $h = 0.9$, $U = -4J$ and $T = 0$. Continuous lines indicate the non-interacting Fermi surfaces, which have identical shapes. For definitions of FB, I-DB, II-DB, refer to the main text of the article.

number of states near the Fermi surface that can pair.

FS DEFORMATION CLOSE TO THE FLAT-BAND SINGULARITY

As we approach the flat band singularity within the η phase on the phase diagram of the Lieb lattice, the deformation of the Fermi surface becomes more and more pronounced. This deformation is such that there be as large a matching as possible between the two FSs. That is where most of the intraband pairing takes place. In Fig. S4 we show four examples of cumulative density for each spin component along the line of $h = 1.05J$. When one of the non-interacting FSs vanishes at the Dirac point, the deformation is most dramatic, and the continuity of the FS is broken, see Fig. S4. The pairing correlations $\langle d_{\mathbf{k}n\uparrow} d_{(\mathbf{q}-\mathbf{k})m\downarrow} \rangle$ in the band basis, as pre-

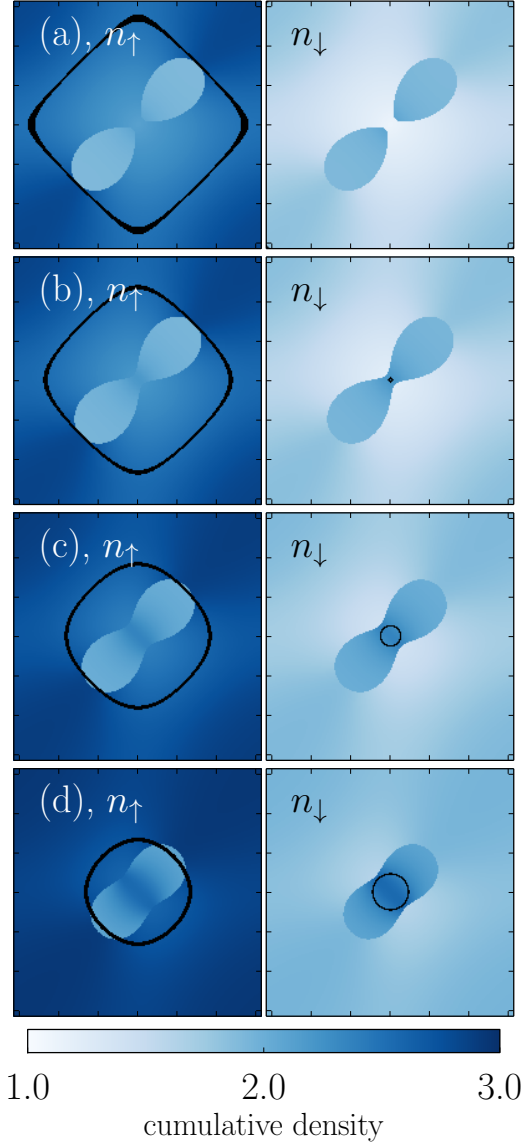


FIG. S4: Total densities of each spin component for four different parameters. The shape of the deformed Fermi surface is revealed by the distribution of the normal part, as it changes within the η phase as we move towards the crossing of the flat band and the Van Hove singularity, i.e. along the line of $h = 1.05J$; Subsequent panels are for (a) $\mu = J$, (b) $\mu = 1.1J$, (c) $\mu = 1.3J$, (d) $\mu = 1.5J$. Since the I-DB is completely filled, the color scale was truncated to the range from 1 to 3 (in the units of the inverse lattice constant a^{-1}).

sented in Fig. S5, show the same mechanism as described in the main text for the generic FF phase: intraband pairing is mostly concentrated within the II-DB and within the flat band, and the interband pairing between the flat band and the II-DB. The difference is that the deformed FS in the η phase is symmetric with respect to the Γ point; this is due to the four-fold symmetry of the original, non-interacting FSs around the said point and to the relative shift of these FSs by the vector $(\pi/a, \pi/a)$.

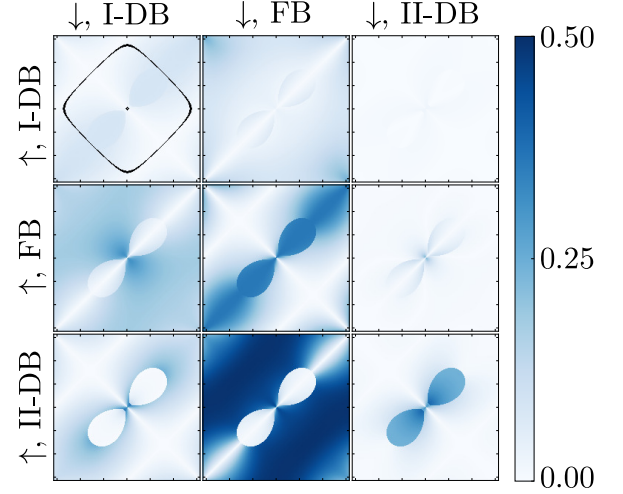


FIG. S5: Correlations corresponding to the densities in Fig. S4(a), i.e. for $h = 1.05J$ and $\mu = J$. The dramatic deformation of the Fermi surface allows for an effective intraband pairing in the II-DB. Like in the generic FF case presented in the main text, there is a large region of interband pairing between the flat band and a II-DB and some residual intraband pairing within the flat band. For definitions of FB, I-DB, II-DB, refer to the main text of the article.

-
- [S1] P. Kumar, T. I. Vanhala, and P. Törmä, *Phys. Rev. B* **96**, 245127 (2017).
 - [S2] T. Maier, M. Jarrell, T. Pruschke, and M. H. Hettler, *Rev. Mod. Phys.* **77**, 1027 (2005).
 - [S3] E. Gull, A. J. Millis, A. I. Lichtenstein, A. N. Rubtsov, M. Troyer, and P. Werner, *Rev. Mod. Phys.* **83**, 349 (2011).